A Prismatic-Revolute-Revolute Joint Hand for Grasping From Unmanned Aerial Vehicles and Other Minimally Constrained Vehicles

Spencer B. Backus[1]
School of Engineering and Applied Science,
Yale University,
9 Hillhouse Avenue,
New Haven, CT 06511
e-mail: spencer.backus@yale.edu

Aaron M. Dollar
Mem. ASME
School of Engineering and Applied Science,
Yale University,
P.O. Box 208284,
New Haven, CT 06520
e-mail: aaron.dollar@yale.edu

Here, we present the design, fabrication, and evaluation of a prismatic-revolute-revolute joint hand called the model B that we developed for grasping from ungrounded vehicles. This hand relies on a prismatic proximal joint followed by revolute distal joints in each finger and is actuated by a single motor- and a tendon-based underactuated transmission. We evaluate this design's grasping capabilities both when fully constrained by a robotic arm and when minimally constrained and evaluate its performance in terms of general grasping capabilities and suitability for aerial grasping applications. The evaluation shows that the model B can securely grasp a wide range of objects using a wrap grasp due to the prismatic-revolute-revolute joint finger kinematics. We also show that the prismatic proximal joints and between finger coupling allows the hand to grasp objects under large positional uncertainty without exerting large reaction forces on the object or host vehicle. [DOI: 10.1115/1.4038975]

Introduction

The types and applications of autonomous unmanned aerial vehicles (UAVs) have proliferated during the last decade from an expensive niche product used primarily by the military or found in research labs to an affordable consumer product. To date, most UAV designs and applications have focused on remote observation and sensing, ranging from large fixed wing drones for military surveillance to small quad rotors used for cinematography and now even personal photography. However, applications where the vehicle physically interacts with the environment such as picking up or delivering an object to a predetermined location represent a significant new and as yet uncommon capability for UAVs [1]. So far, researchers have demonstrated UAVs transporting cargo, picking up objects, perching on features in the environment, and even manipulating objects while in flight using a multi-link arm [2–25].[2] However, all of these systems have relied on structuring the interaction problem, simple single purpose grippers, or slight adaptations of existing hands that are not intended for this application.

Furthermore, the majority of grasping and manipulation research has focused on stable robotic platforms where the robot is either fixed in the environment or massive in comparison to the objects being manipulated, and therefore, behaves as though it is fixed in space [1,26,27]. Although this paradigm applies to hands designed for many existing robotic applications such as industrial robotic arms and terrestrial mobile robots, it is not the case when grasping from a flying, underwater, or space vehicles. Unlike large or fixed platforms, these vehicles are easily perturbed by external forces, and in comparison to a ground vehicle, can be more difficult to position or maintain a pose during grasp acquisition. Therefore, we set out to design a hand specialized for aerial, underwater, or space grasping that can grasp a wide range of objects while minimizing the grasp reaction forces and maximizing the allowable pose error.

In this paper, we present the design, fabrication, and evaluation of a prismatic-revolute-revolute joint hand developed for grasping from aerial vehicles that is shown in Fig. 1. This design builds upon the experience gained from the design and analysis of hands with related kinematic and our understanding of the design requirements for the aerial grasping application that it is intended for [28–30]. We begin by describing the kinematics of the hand that we built based on the previously presented optimization results [30]. Next, we describe the actuation of the hand, including the between joint coupling scheme, force allocation, and physical implementation of these design choices. We then describe how the prototype was fabricated and evaluated. Evaluation of the hand included measuring its grasp strength, grasp reaction force, and object reconfiguration trajectory as well as evaluating its grasping capabilities and tolerance of positional error when fully constrained by a robotic arm and when minimally constrained using the Yale–CMU–Berkeley (YCB) object set. Finally, we discuss how the hand performed on these tests and how this performance relates to the use of the hand as an aerial grasper.

Hand Design

We begin by describing the general configuration of the hand and the motivation for developing this particular kinematic configuration. Previous modeling of a two-joint revolute finger hand showed the impact of palm spacing (the distance between the two proximal revolute joints) on grasp performance and how it related to object size [29]. Similarly, our experience with the performance of the model S hand prototype demonstrated the utility of a hand

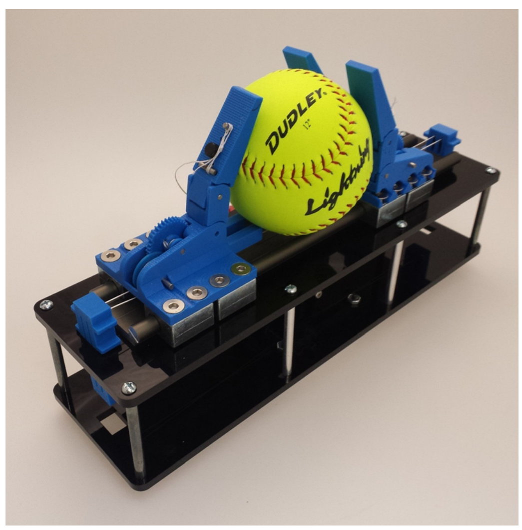

Fig. 1 The model B hand, shown grasping a softball. The prismatic joints allow the finger spacing to adjust to the size of the object, while the revolute joints allow the fingers to wrap about the object.

[1]Corresponding author.
[2]Amazon Prime Air, https://www.amazon.com/Amazon-Prime-Air/b?ie=UTF8&node=8037720011

Manuscript received September 24, 2017; final manuscript received December 14, 2017; published online February 5, 2018. Editor: Venkat Krovi.

 Copyright © 2018 by ASME

Downloaded From: http://mechanismsrobotics.asmedigitalcollection.asme.org/ on 03/02/2018 Terms of Use: http://www.asme.org/about-asme/terms-of-use

that combines prismatic and revolute joints in series in each finger [28]. Building upon these results, in this paper, we describe and evaluate a hand that combines elements of multilink revolute and prismatic joint hands. It consists of opposed P-R-R joint underactuated fingers as shown in Fig. 2. The main justification behind this configuration is outlined in Fig. 3: typical hand configurations will regularly produce a net outward force on objects during acquisition, which would serve to push the vehicle away from the object in ungrounded/minimally constrained scenarios such as aerial, underwater, or space applications. Instead, we are considering a configuration that would only apply mostly inward forces to the object during the acquisition process.

We believe that this combination of prismatic and revolute joints effectively adds a variable size palm to the hand, allowing it to adapt to the size of the object. However, unlike a purely prismatic joint hand, the addition of multilink revolute joint fingers increases the hand's ability to conform to objects and the strength of the resulting grasp. Finally, actuation and control complexity can still be minimized by actuating all of the joints with a single actuator and underactuated transmission that exerts a force (F_T) on the prismatic joint and proportional torques ($\tau_1 = F_T R_1$, $\tau_2 = F_T R_2$) about the revolute joints.

We also selected this hand morphology since aspects of its grasping behavior are desirable when grasping from a UAV. Unlike a purely revolute joint hand, the P-R-R joint kinematics and initial joint configuration of the fingers perpendicular to the palm ensure that fingertip motion is parallel to or toward the palm of the hand when grasping. This constraint on the fingertip trajectory means that contact forces on the grasped object arising from the closing motion of the hand will push the object further into the grasp, thereby reducing the chance of the hand inadvertently knocking the object out of the hand prior to the acquisition of a secure grasp. Similarly, this fingertip trajectory ensures that actuation of the hand will not result in unexpected contact with the environment that may push the hand away from the desired position or generate unexpected normal reaction forces on the vehicle. Furthermore, the between finger coupling implemented in this design means that similar contact forces will be exerted on an object wherever it is positioned laterally in the hand's workspace and ensures that minimal force will be exerted on the object until both fingers make contact. This feature improves the hand's tolerance of positional error and minimizes the lateral reaction forces exerted on the vehicle during grasp acquisition. Finally, the within finger underactuation allows the fingers to conform to the object after both fingers make contact, improving the robustness of the resulting grasp.

The variable palm width of the P-R-R hand morphology also contributes to the positional error tolerance of this design since it facilitates the initial pose of the hand consisting of widely spaced opposing fingers normal to the palm. This initial configuration of the hand ensures a large approach volume (defined as the convex polyhedron inscribed between the fingers and the palm) and approach area (the polygon inscribed between the fingertips [31]) for a given palm width and finger length. The large approach area allows for large positional errors when approaching the object, while the large grasp volume allows the object to be caged by the gripper prior to contact. In comparison, hand designs built with revolute joint fingers and a fixed palm width often have closely spaced proximal joints and widely opened fingers that result in a large approach area but small approach volume. This combination is undesirable when attempting to grasp with high positional error while still minimizing pregrasp contact forces since objects may contact the palm before they are fully caged by the fingers.

Kinematics. We set out to construct a three-finger interdigitating hand with prismatic-revolute-revolute joint fingers based upon the optimization work described in Ref. [30]. The hand has link length ratios of 0.18, 0.24, and 0.58 for the proximal, intermediate, and distal links and intermediate and distal joint moment arms equal to approximately 0.95 times the length of the digit distal to the respective joint. Based upon an overall finger length of 100 mm, this results in a finger with an 18 mm proximal link, 24 mm intermediate link, and 58 mm distal link. The prismatic joint has 180 mm of travel, slightly less than two times the finger length. Each finger is 20 mm wide and the adjacent fingers are spaced 24 mm apart, allowing the opposing finger to pass between them when flexed. Finally, the finger pad surface is 7.5 mm in front of the joint axis on all three links. These dimensions attempt to balance the desire to make the hand compact and the space needed to incorporate elements like pulleys and springs in the fingers.

Actuation. As described in Ref. [30], this hand is designed to be actuated in such a way that actuator force is equally applied to

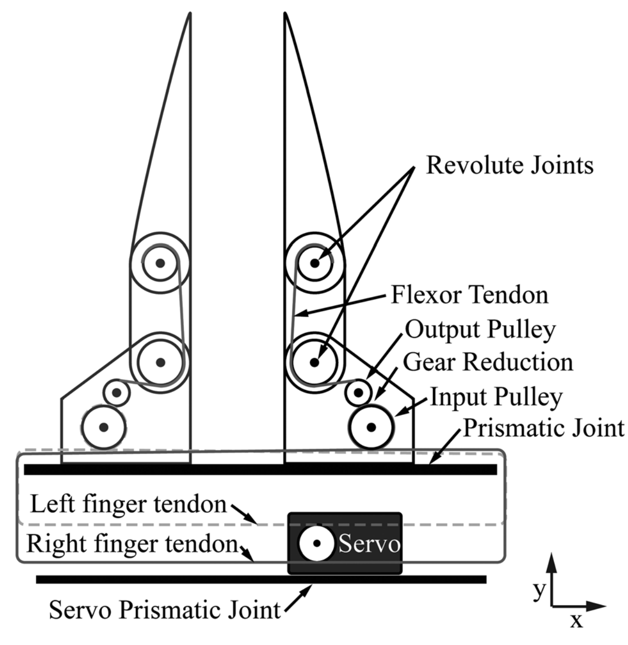

Fig. 2 Diagram of the finger kinematics that shows the prismatic and revolute joints of the finger as well as the tendon routing and gear reduction from the servo to the finger

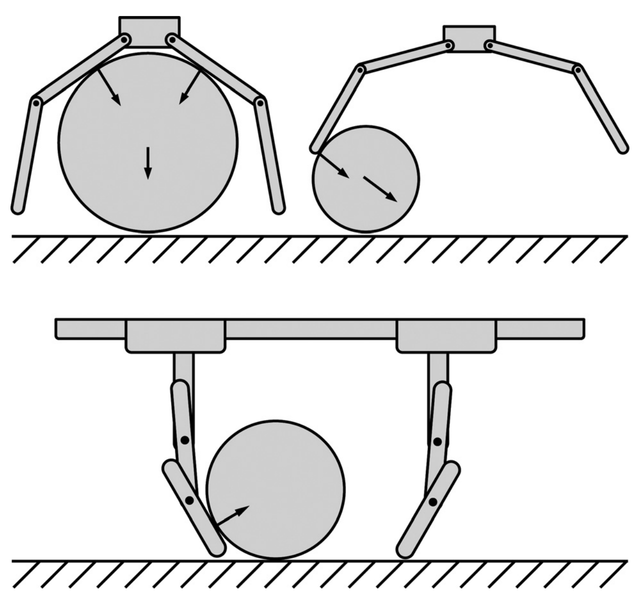

Fig. 3 Diagram of the finger kinematics that shows the prismatic and revolute joints of the finger as well as the tendon routing and gear reduction from the servo to the finger

Downloaded From: http://mechanismsrobotics.asmedigitalcollection.asme.org/ on 03/02/2018 Terms of Use: http://www.asme.org/about-asme/terms-of-use

each finger and proportionally to the prismatic and revolute joints. Furthermore, based upon the moment arm optimization results, if a specific force is applied to the prismatic joint, the torques applied to the revolute joints should be equal to this force times the length of the finger distal to each joint. This actuation scheme ensures that the fingers will center about the object regardless of where it is positioned along the prismatic joint and that once the fingers make contact, they will wrap about the object, pulling it further into the grasp.

However, directly implementing this actuation scheme is impractical since the radii of the desired tendon moment arms (82 mm for the distal joint and 58 mm for the proximal joint) would extend past adjacent joints. Instead, we built the fingers with much smaller but proportional joint moment arms (6.35 mm and 4.5 mm) and added a gear reduction between the tendons actuating the prismatic and revolute joints as shown in Fig. 2. The total reduction provided by this gear box can be calculated as follows: $F_{\text{out}} = (N_2/N_1)(r_1/r_2)F_{\text{in}}$, where N_1 and N_2 are the number of gear teeth and r_1 and r_2 are the radius of the input and output pulleys, respectively. As constructed, $N_1 = 14$, $N_2 = 60$, $r_1 = 9$ mm, and $r_2 = 3.175$ mm, resulting in an overall ratio of 12.13. This results in effective joint moment arms of approximately 0.95 times the finger lengths, much larger than would be feasible without the gear reduction.

Extension of the revolute joints of each finger is achieved via weak torsion springs (0.0145 N·m/rad) encapsulated in the joints that are just stiff enough to extend the respective joints when the flexion tendon is slack. Soft springs were selected to minimize the amount of actuator force required to overcome the springs while grasping. Unlike the revolute joints, extension of the prismatic joint is achieved via an antagonist tendon as shown in Fig. 2. This extension tendon is wound the opposite way around the input pulley at the base of the finger and the servo pulley as the prismatic actuation tendon, effectively forming a continuous loop. When the hand closes, the flexor tendon is pulled in, while the extensor tendon is paid out an equal amount. Depending on how the finger is constrained, commanding the finger to flex will cause the prismatic joint to translate, the input pulley to the finger to rotate and flex the revolute joints, or some combination of the two. Driving the servo in the other direction pulls the extension tendon, rotating the pulley until the revolute joints are fully extended. At this point, the pulley contacts a hard stop that prevents further rotation and the tendon directly actuates the prismatic joint, causing it to open. This active actuation of both the opening and the closing of the prismatic joint ensures that the joint open consistently regardless of joint friction and that closure force is constant for all finger positions unlike hands that rely on an antagonist joint springs.

The hand is composed of three fingers arranged so that the finger on one side is capable of interdigitating between the opposite two. To ensure that the hand applies equal force to either side of the object when grasping, each of the two adjacent fingers is actuated with half the force of the single opposing finger. This is achieved by connecting the adjacent fingers' prismatic bases and the input pulleys to each finger's gearbox and actuating them both with a single prismatic joint tendon. Finally, the single and opposing pair of fingers are actuated by the same motor. The prismatic flexion/extension tendon loops for each finger are wrapped in opposite directions around a pulley on the servo output so that all three fingers are simultaneously either flexed or extended when the servo rotates as illustrated in the diagram in Fig. 2. In order to allow for between finger adaptability, the motor is mounted on a linear bearing parallel to the tendons. This joint is equivalent to driving the two tendon outputs via a differential and a single actuator but proved to be easier to implement.

Fabrication. Based upon these design decisions, we have built a prototype of the hand using methods derived from the Yale OpenHand Project [32]. The body of the hand is made from laser cut 0.25 in (0.635 cm) acrylic, 2.5 in (6.35 cm) long steel standoffs, and three-dimensional (3D)-printed acrylonitrile butadiene styrene (ABS) plastic components (printed on a Fortus 250mc). The fingers are also 3D-printed. Revolute joints are implemented with 0.125 in (0.3175 cm) steel dowel pins that are press fit into the proximal element and pass through oversized (slip fit) holes in the distal element of each joint. A steel torsion spring (McMaster Carr 9271K94) is used as return springs for the revolute joints in each finger. This spring is preloaded to resist finger flexion until the finger contacts and object. The reduction gear box in each finger is composed of molded nylon gears (SDP/SI A1N 1-N48060 and A 1N 2-N48014) and 3D printed drums rotating on 1/8 in (0.3175 cm) steel pins in a 3D printed housing. The prismatic joints of the fingers and actuator are constructed using off-the-shelf linear bearings (Igus TK-04-09 and WS-10-40). A Robotis Dynamixel MX-64 servo operating at 12 V is used to actuate all three fingers directly via 150-lb test Spectra fishing line tendons routed across 0.375 in (0.9525 cm) acetal pulleys.

Gripper Evaluation Procedure

This hand has been evaluated in a number of different ways to compare its capabilities to other designs as well as to evaluate its suitability for aerial grasping tasks. First, we quantify aspects of its grasping behavior by measuring the object reaction forces throughout the hand's workspace as well as the object's trajectory from the initial contact until a grasp is achieved. To facilitate comparison to other hands, we also report the hand's basic specifications and characterize its performance via the YCB object set gripper assessment protocol and modified NIST slip resistance tests [33–36]. Finally, we demonstrate the hand's suitability for aerial grasping tasks by demonstrating its grasping capabilities when suspended by a compliant tether. Although demonstrating the hand's grasping capabilities from a UAV in flight would be desirable, we have not been able to perform any vehicle-based tests due to the restrictions imposed on UAV operation by the Federal Aviation Administration (FAA) during the last few years.

In order to predict the behavior of the system when grasping light objects that are easily perturbed or fixed objects that could perturb the vehicle, we measure the object hand reaction force: the force applied to the object during the grasp when both the hand and the object are fixed relative to each other. This test condition measures the highest possible force that the vehicle may experience when grasping a large object or a fixed object when perching. To measure the grasp reaction forces, we mounted an ABS plastic cylinder to a six-axis load cell (ATI Gamma F/T sensor) that is fixed in place relative to the hand. The axis of the cylinder is aligned with the z-axis of the load cell and the y-axis is normal to the palm of the hand. The hand is then commanded to close (servo torque is set to 20), while the load cell records the forces applied to the object. This procedure is then repeated at 0.5 in (1.27 mm) increments in the y direction at the center of the hand's lateral workspace. This test is repeated with the object positioned ± 1.5 in (3.81 cm) and ± 2.5 in (6.35 cm) to either side of the center in the x direction, thereby sampling the reaction force throughout the hand's workspace. We then report the magnitude of the largest observed lateral and normal force at each sampled location.

We also measure the trajectory of an unconstrained object (an ABS plastic cylinder) in the hand as the fingers close and relate it to the positional error tolerance of the hand. To measure the unconstrained object's trajectory, the hand is fixed in space and the object is tracked, while it is grasped via a camera and fiducial. This procedure is repeated at approximately 10 mm increments in the Y direction at the center of the hand's lateral workspace and ± 40 and ± 60 mm to either side of it in the X direction. Each initial position is then categorized based on if the object is pulled toward the hand, pinched between the fingertips, or ejected from the grasp.

Although the overall procedure for executing the NIST and YCB tests is the same as that described in Ref. [28], certain elements of these tests are altered to accommodate and evaluate

Downloaded From: http://mechanismsrobotics.asmedigitalcollection.asme.org/ on 03/02/2018 Terms of Use: http://www.asme.org/about-asme/terms-of-use

specific aspects of this hand's design and intended use. These modifications to the procedure are described here. First, we altered the NIST slip resistance metric to accommodate this hand design. When the test cylinder is centered in the grasp, it is anchored via two parallel tendons (one on either side of the grasp) instead of a single tendon that would have to pass through the middle finger because the fingers interdigitate. Second, to prevent damage to the hand when conducting this test, the servo torque is only set to 25 via the DYNAMIXEL WIZARD software and tests are terminated when the object is pulled from the hand or the load applied to the hand exceeds 200 N. When conducting the YCB tests, the X axis is parallel to the prismatic joint, the Y axis is perpendicular to the prismatic joint, and the Z axis is normal to the palm of the hand. In addition to testing the hand at the set points specified in the procedure, we also offset each object by -1 cm in the X and Y directions.

Finally, in order to demonstrate the hand's grasping abilities when minimally constrained, as will be the case when attached to a UAV, we also demonstrate the hand grasping the same set of objects used in the YCB gripper assessment protocol (excluding those that could not be grasped under any conditions) when it is suspended via a compliant tether (note that we are not certified to test on aerial vehicles under current FAA regulations). The hand is suspended via a 30 cm long loop of spectra line from the vertically mounted linear actuator with 4 in (10.16 cm) of travel (ServoCity HDLS-4-50-12V). When the actuator is fully retracted, the finger tips are 7 cm above the surface and when fully extended the hand rests on the ground surface with the fingers partially flexed. During a test, the object is placed at the target position centered below the hand on a smooth sheet of acrylic and the hand is then lowered until the actuator is fully extended. The hand is then closed (servo torque is set to 20). After the actuator stalls, the hand and the grasped object are lifted clear of the ground by fully retracting the linear actuator. If the object remains in the hand and is lifted off the ground, the grasp is judged to have succeeded.

This test is repeated with the object offset relative to the initial configuration by ± 5 cm in X and Y and $+2.5$ cm in Z (where the fingertips just touch the surface) in order to evaluate positional error tolerance. The test is also repeated with the object at the target position but with the ground surface rotated ± 7.5 deg about the X and Y axes to assess the effect of the hand and ground not being aligned. In these trials, the round objects are placed on various sized washers with rubber feet to keep the objects from sliding or rolling down the sloped surface before they can be grasped. When needed, the washers or small pieces of rubber were also used to keep the tools from moving. In all cases, each grasp trial is repeated three times to gauge the repeatability of the configuration and the number of successes is reported. To help compare the hand's performance at various set points and for different classes of objects, the total number of successful grasps for each object class at each set point and overall are also tallied.

Results and Discussion

Object Hand Reaction Force. Figure 4 shows the object hand reaction force results for the hand grasping a 3 cm diameter cylinder throughout the hand's workspace when the servo torque is set to 20. Figure 4(*a*) shows the maximum (or minimum when negative) lateral (left/right) force at each point sampled in the workspace, while Fig. 4(*b*) shows the maximum (or minimum when negative) normal force where positive is defined as away from the palm of the hand. As shown in Fig. 4(*a*), the maximum lateral force is approximately 10 N and is applied when the object is near the palm and at the extreme left or right edge of the workspace. The lateral force is exerted to overcome the friction within the prismatic finger joints and differential mechanism. However somewhat surprisingly, the lateral force varies with the distance of the object from the palm and is highest when the object is near the palm at the extreme left or right edge of the workspace. This is a direct result of the friction in the prismatic joint causing the finger

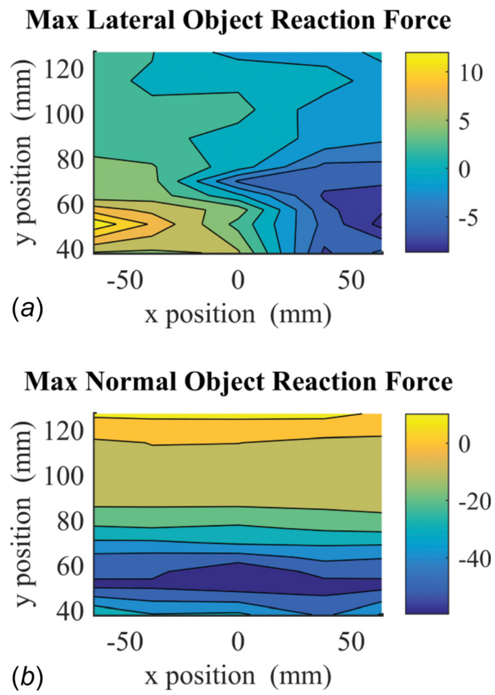

Fig. 4 Object hand reaction force in Newtons when grasping 3 cm diameter cylinder. Subfigure (*a*) shows the maximum lateral force where positive force is to the right. Subfigure (*b*) shows the maximum normal force where positive is up, away from the palm of the hand.

to flex in addition to translating: since the object contact force is then resisting a joint moment, the closer the contact point is to the joint the higher the contact force. When the object moves even closer to the palm, the lateral force is reduced since the object is then contacting the proximal prismatic link, not the revolute intermediate link.

Figure 4(*b*) shows that the maximum normal reaction force is predominantly affected by the distance of the object from the palm. At the edge of the workspace, furthest from the palm, the normal component of the reaction force is away from the palm and pushes the object out of the grasp. As the object moves closer to the palm, the normal reaction force direction switches and then increases until it reaches a maximum of approximately 55 N when the object is 5 cm from the palm of the hand. The reaction force drops slightly when the object is only 4 cm from the palm since the forces applied to the object deflects it enough that it contacts the palm from this position. Although we expect to see this general trend regardless of the magnitude of the commanded servo torque, increasing or decreasing the motor torque should proportionally increase or decrease the normal reaction force throughout the workspace while having minimal impact on the lateral reaction forces. This decoupling of lateral and normal reaction forces is desirable for aerial grasping since it minimizes lateral forces that may destabilize the vehicle or affect its station keeping while allowing high vertical forces to be exerted drawing the object into the grasp or the vehicle onto a perch.

In Hand Object Motion. Figure 5 shows the expected in hand object motion for the hand gripping a 4 cm diameter cylinder that weighs 220 g. As we expect from the reaction force results, when positioned near the edge of the workspace, the object is pushed out (dashed gray trajectories) and when closer to the palm, the object is pulled into the grasp (solid gray trajectories). Between these two regions, the object is simply pinched between the fingertips (black trajectories). Also, as can be seen in the various recorded trajectories, even when offset laterally from the center of the hand, the object is primarily displaced in or out of the hand, not side to side. Lateral motion occurs when the contact force

Downloaded From: http://mechanismsrobotics.asmedigitalcollection.asme.org/ on 03/02/2018 Terms of Use: http://www.asme.org/about-asme/terms-of-use

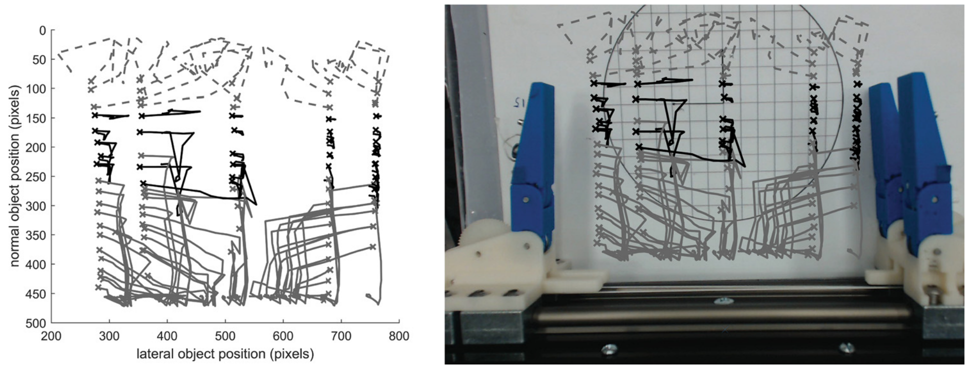

Fig. 5 Object motion when grasping a 4 cm diameter cylindrical object that weighs 220 g. The figure (left) shows motion trajectories that are coded based on if the object is pulled into a wrap grasp (solid gray lines), pinched between the fingertips (solid black lines), or ejected (dashed gray lines). The starting position is plotted with *x*, while the end position is indicated by a dot. The same trajectories are also overlaid over an image of the hand in the open position (right).

Table 1 Hand pullout strength

1 in tube, centered		1 in tube, offset		2 in tube, centered		2 in tube, offset	
Mean	Deviation	Mean	Deviation	Mean	Deviation	Mean	Deviation
>200 N	NA	49.4 N	5.8 N	119.9 N	5.1 N	35.2 N	1.9 N

Table 2 Scoring table for YCB gripper assessment

				X		*Y*		*Z*
	Object	Size (cm)	Target	+1 cm	−1 cm	+1 cm	−1 cm	−1 cm
Round objects	Soccer ball	ø14.5	4	4	4	4	4	4
	Softball	ø9.5	4	4	4	4	4	4
	Tennis ball	ø6.5	4	4	4	4	4	4
	Racquetball	ø5.5	4	4	4	4	4	4
	Golf ball	ø4.27	4	4	4	4	4	4
	Marble (XL)	ø3.54	4	4	4	4	4	4
	Marble (L)	ø2.41	0	0	0	0	0	0
	Marble (M)	ø2.22	0	0	0	0	0	0
	Marble (S)	ø1.74	0	0	0	0	0	0
Flat objects	Washer 1	ø5.08 × 0.37	4	4	4	4	4	NA
	Washer 2	ø3.73 × 0.27	4	4	4	4	0	NA
	Washer 3	ø3.16 × 0.12	0	0	0	0	0	NA
	Washer 4	ø2.53 × 0.17	0	0	0	0	0	NA
	Washer 5	ø1.88 × 0.19	0	0	0	0	0	NA
	Washer 6	ø1.29 × 0.13	0	0	0	0	0	NA
	Washer 7	ø0.98 × 0.13	0	0	0	0	0	NA
	Credit card	8.55 × 5.4 × 0.075	4	4	4	4	4	NA
Tools	Pen	Sharpie	4	4	4	4	4	0
	Scissors	3.5 in blade	4	4	4	4	4	0
	Hammer	13 oz stanley	4	4	4	4	4	4
	Screwdriver	Stanley philips	4	4	4	4	4	4
	Drill	Black&Decker	3	3.5	3.5	3.5	3.5	3
	Peg XL	Nylon clamp	4	4	4	4	4	4
	Peg L	Nylon clamp	4	4	4	4	4	4
	Peg M	Nylon clamp	4	4	4	4	4	0
	Peg S	Nylon clamp	4	4	4	4	4	0
Articulated	Chain	117 cm long	6/20	NA	NA	NA	NA	NA
	Rope	353 cm long	20/20	NA	NA	NA	NA	NA
		Target, +*x*, +*y*, −*z*						
Score	Round object:	96/144	24/36	24	24	24	24	24
	Flat objects:	36/96	12/32	12	12	12	8	NA
	Tools:	125/144	35/36	35.5	35.5	35.5	35.5	19
	Articulated:	13/20	13/20	NA	NA	NA	NA	NA
	Total:	270/404	71/104	71.5	71.5	71.5	67.5	43

Downloaded From: http://mechanismsrobotics.asmedigitalcollection.asme.org/ on 03/02/2018 Terms of Use: http://www.asme.org/about-asme/terms-of-use

required to overcome the sliding friction between the object and the ground is less than the force needed to overcome the friction in the hand's between-finger differential mechanism. Therefore, lateral motion is only observed when grasping light weight objects or when the object is on a low friction surface. In this case, the weight and frictional properties of the object are near the transition point between the domains where internal hand friction and object friction dominating so in some cases the hand reconfigures before the object moves, and in other instances, the object slides laterally until both fingers make contact.

Grasp Strength. Table 1 summarizes the measured grasp strength of this hand as measured by the modified NIST slip resistance test. As can be seen from these results, this hand is capable of grasping and lifting heavy objects but the grasp strength is somewhat sensitive to both object size and loading condition. In the centered test condition, the hand could exert about 120 N on the 2 in (5.08 cm) diameter cylinder before it was pulled out of the grasp. In comparison, the test was stopped when the load exceeded 200 N in all five trials when grasping the smaller 1 in (2.54 cm) diameter cylinder. A similar relationship between grasp strength and object diameter exists for the offset test condition: the hand exerts approximately 1.4 times more force on the 1 in (2.54 cm) cylinder than on the 2 in (5.08 cm) cylinder before they are each pulled from the grasp. Finally, the pull out strength of the grasp decreases significantly between the centered and offset conditions for both diameter cylinders that were tested. When the load is centered in the grasp, the fingers must be flexed open before the grasp fails. In the offset case, the moment applied to the object rotates it and then the force pulls it axially out of the grasp. Since the test objects are made from polyvinyl chloride and finger surfaces are made from smooth ABS, the coefficient of friction between them is relatively low and the grasp is unable to resist large axial forces on the object. Therefore, adding high friction grip pads may improve the grasp strength, particularly for the offset loaded case.

Yale–CMU–Berkeley Object Set Gripper Assessment. Table 2 summarizes the performance of the hand on the YCB object set gripper assessment and at the additional set points that were tested. In this table, we report the hand's scores for individual objects at each set point, sub scores for each class of object at each set point and overall score. Overall, the hand scored 270 out of 404 possible points. In general, the hand performs well for all of the test objects except the very small ones. This is because the gap between the adjacent fingers (that allows for interdigitation) is 2.45 cm, with the size of the hand and finger spacing making it essentially only appropriate for objects of approximately 3.5–14.5 cm in diameter in the grasped plane. Another weakness of the design is that heavy objects, such as the drill, often shift when reoriented due to the low friction ABS finger surfaces—an issue that can be improved with a high-friction fingerpad.

Tethered Grasping. Table 3 summarizes the tethered grasping performance of the hand. In this table, we report the number of successful grasps out of three consecutive attempts for individual objects at each set point (target, ± 5 cm in X, ± 5 cm in Y, $+2.5$ cm in Z, ± 7.5 deg about X, and ± 7.5 deg about Y) as well as the total number of successful grasps for each set point and class of objects. We also show examples of a few successful and failed grasp trials at various set points in Fig. 6. In general, these results show that when only supported by the tether, the hand is incapable of grasping thin objects (due to lack of sufficient forces to keep aligned with the table surfaces) but can still robustly grasp many round objects, tools, and articulated objects from the object set. The results also show that the grasps are tolerant to positional error and lack of alignment with the ground surface but that this is somewhat dependent on both the object and the direction of the error.

The overall results for the tethered hand show variability based on a number of factors related to the design of the hand and the direction of the positional error. When grasping objects at the

Table 3 Tethered gripping performance

				X		Y		Z	X		Y	
	Object	Size (cm)	Target	$+5$	-5	$+5$	-5	$+2.5$	$+7.5$ deg	-7.5 deg	$+7.5$ deg	-7.5 deg
Round objects	Soccer ball	ø14.5	3/3	NA	NA	0	0	3/3	3/3	3/3	3/3	3/3
	Softball	ø9.5	3/3	NA	NA	0	0	3/3	3/3	3/3	3/3	3/3
	Tennis ball	ø6.5	3/3	0	3/3	0	0	3/3	3/3	0	2/3	2/3
	Racquetball	ø5.55	1/3	0	3/3	0	0	2/3	3/3	0	0	1/3
	Golf ball	ø4.27	1/3	1/3	3/3	0	0	2/3	3/3	0	0	0
	Marble (XL)	ø35.4	3/3	0	3/3	0	0	2/3	3/3	0	0	0
Flat objects	Washer 1	ø5.08 × 0.37	0	0	0	0	0	0	0	0	0	0
	Washer 2	ø3.73 × 0.27	0	0	0	0	0	0	0	0	0	0
	Credit card	8.55 × 5.4 × 0.075	0	0	0	0	0	0	0	0	0	0
Tools	Pen	Sharpie	3/3	3/3	3/3	0	0	3/3	3/3	3/3	0	2/3
	Scissors	3.5 in blade	3/3	3/3	3/3	1/3	3/3	3/3	3/3	0	2/3	0
	Hammer	13 oz stanley	3/3	3/3	3/3	3/3	3/3	3/3	3/3	3/3	1/3	2/3
	Screwdriver	Stanley philips	3/3	3/3	3/3	3/3	3/3	3/3	3/3	3/3	1/3	3/3
	Drill	Black&Decker	3/3	3/3	3/3	3/3	3/3	3/3	3/3	3/3	3/3	2/3
	Peg XL	Nylon clamp	3/3	3/3	3/3	0	3/3	3/3	3/3	2/3	3/3	3/3
	Peg L	Nylon clamp	3/3	0	3/3	0	0	3/3	2/3	3/3	3/3	2/3
	Peg M	Nylon clamp	2/3	0	3/3	0	0	3/3	1/3	2/3	2/3	1/3
	Peg S	Nylon clamp	2/3	0	1/3	0	0	1/3	1/3	3/3	2/3	0
Articulated	Chain	1168 mm long	1/3	NA	NA	NA	NA	2/3	1/3	0/3	2/3	3/3
	Rope	3530 mm long	3/3	NA	NA	NA	NA	3/3	2/3	2/3	2/3	3/3
		All conditions										
Score	Round object:	83/180	14/18	1	12	0	0	15	18	6	8	9
	Flat objects:	0/90	0/9	0	0	0	0	0	0	0	0	0
	Tools:	194/270	25/27	18	25	10	15	25	22	22	17	15
	Articulated:	24/36	4/6	NA	NA	NA	NA	5	3	2	4	6
	Total:	301/576	43/60	19	37	10	15	45	43	30	29	30

Downloaded From: http://mechanismsrobotics.asmedigitalcollection.asme.org/ on 03/02/2018 Terms of Use: http://www.asme.org/about-asme/terms-of-use

target, success or failure is primarily dependent on how the initial contact causes the object to move as the hand continues to close. Grasps of round objects fail when the initial contact (often from the single finger) causes them to roll out of the grasp. Similarly, grasps of the tools at the target position fail when the initial contact causes the object to slide or rotate into an undesirable configuration relative to the hand. This primarily affected grasps of the smaller tools (the size M and S pegs) that were sensitive to less than ideal object position. In contrast, the greater size of the larger tools made them easier to grasp from slightly different positions and their increased weight made them less likely to be shifted by the initial contact with the hand.

The hand exhibits significant reduction in grasp success when the objects are displaced in the positive and negative X directions (largely due to contact force imbalance), and worse when objects are displaced in Y (largely due to the size of the graspable surface of the objects being out of reach). The results also show that moving the hand up 2.5 cm in Z away from the grasp surface shows comparable performance to the normal condition (actually two more successful grasps). Furthermore, angling the grasp surface relative to the hand has minimal impact on the hand's performance when the ground is angled $+7.5$ deg about X but moderately reduces its grasp success when angled -7.5 deg about X or either direction about Y.

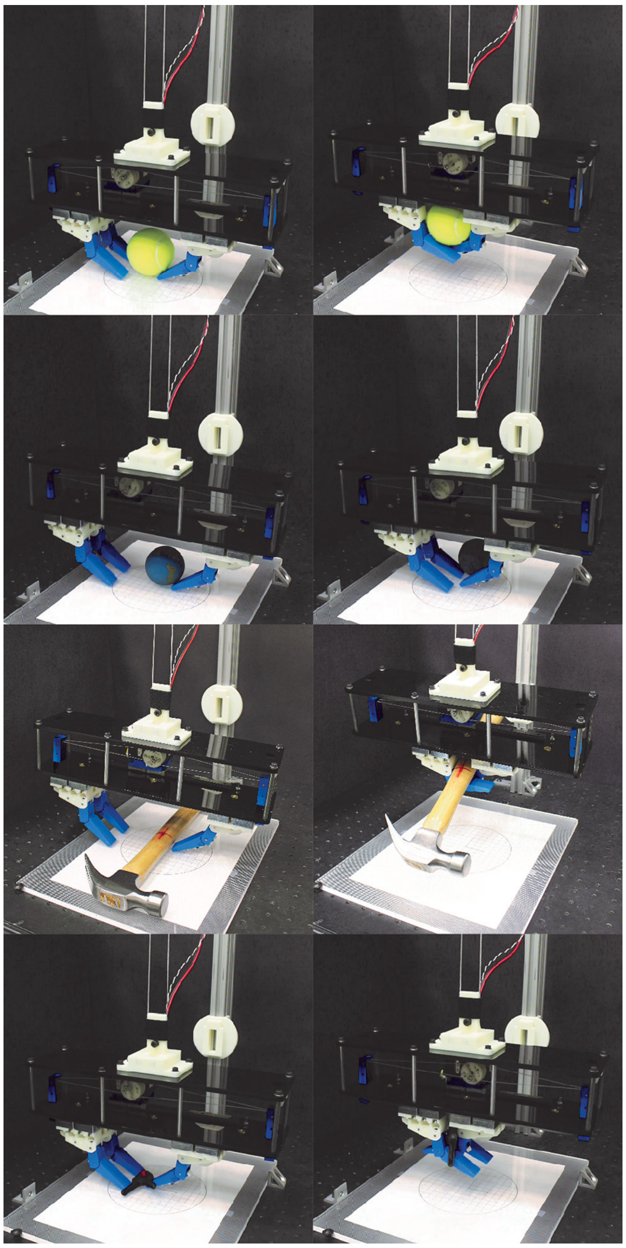

Fig. 6 Examples of successful (tennis ball and hammer) and unsuccessful (racquet ball and small peg) grasp attempts from the target position

Future Work

While the existing configuration of the model B hand for grasping from ungrounded platforms shows good performance for a range of realistic grasping scenarios, the design can be improved further. In particular, we believe that increasing the number of fingers used in this hand from three to five while preserving the symmetry and interdigitation capabilities will substantially improve the grasp reliability of this design when subject to large positional errors in the Y direction. Adding additional fingers or widening the existing fingers will increase the span of the grasp in this direction, thereby increasing the range of object positions that are between the fingers and can be grasped. Adding additional fingers will also increase the number and spacing of contacts made with an object, increasing the chance that the contacts will push the object into the grasp and improve its grasp performance when subject to positional error in the X direction as well.

Although this hand design performed well in its current form with low friction ABS finger surfaces, experimentation with increasing the coefficient of friction at the contacts by using other finger pad materials may improve the grasp strength further. Using a more compliant and higher friction material will increase the frictional forces a grasp can exert on an object which will increase the strength of a grasp and the resistance to out of plane motion of the object. However, increasing the contact friction may also prevent objects from reconfiguring and being pulled into a secure wrap grasp as the hand closes, reducing the strength of the resulting grasp. Therefore, this experimentation may involve determining the optimal coefficient of friction for the finger pads that maximizes grasp strength while still allowing most objects to reconfigure within the hand as they are grasped. It may also be worth investigating materials with directional frictional properties that would allow grasped objects to easily slide into the hand but resist motion in other directions.

The weight and size of the next iteration of the model B design may also be improved upon without altering its grasping performance by reducing the size of the reduction gearing at the base of the fingers and using a lighter weight and lower friction linear bearing in the prismatic joints of the fingers. Furthermore, a more complex telescopic prismatic joint could be developed to reduce the width of the hand when the fingers are closed.

Although the model B hand was capable of grasping most of the objects tested, the spacing of the interdigitating fingers prevented this design from grasping smaller objects. This limitation may be addressed by altering the design to rely on directly opposed fingers capable of pinching small objects. We expect that this modification will reduce the hand's wrap grasp abilities and grasp strength when grasping smaller diameter objects where the fingertips make contact after wrapping about the object. However, being able to execute a pinch grasp will allow the hand to pick up smaller and thinner objects than the current design is capable of grasping.

Finally, although we have quantified the grasp reaction forces and positional error tolerance as well as demonstrated the hand's general grasping capabilities, we have not tested it on a UAV or other ungrounded vehicle. Although our test results suggest that the hand should perform well when mounted directly to a UAV or suspended below a vehicle on a tether, these tests cannot fully replace actual validation through flight testing. Performing UAV tests with the existing hand prototype should be straightforward since integration of the hand will only require mechanical attachment of the hand to the vehicle, 12 V electrical power and a RS485 control signal to the servo actuator. However, we have not

Downloaded From: http://mechanismsrobotics.asmedigitalcollection.asme.org/ on 03/02/2018 Terms of Use: http://www.asme.org/about-asme/terms-of-use

been able to perform any vehicle-based tests due to the restrictions imposed on UAV operation by the FAA during the last few years.

Conclusions

In summary, while grasping from aerial vehicle has the potential to greatly expand their applications, the existing attempts have been limited by the available end effectors. In this paper, we presented the design of a new hand that attempts to address some of the limitations of current aerial grasping end effectors. Although we believe that the evaluation of this gripper shows its potential for aerial grasping applications, this design is only one possible approach to the challenges posed by aerial grasping. Future efforts to improve the end effectors as well as to understand and improve other components of the Mobile Manipulator-UAV system will lead to the broad implementation and utilization of UAVs to perform many tasks.

Funding Data

- National Science Foundation (Grant No. IIS-1317976).

References

[1] Leutenegger, S., Hürzeler, C., Stowers, A. K., Alexis, K., Achtelik, M. W., Lentink, D., Oh, P. Y., and Siegwart, R., 2016, "Flying Robots," *Springer Handbook of Robotics*, B. Siciliano and O. Khatib, eds., Springer International Publishing, Cham, Switzerland, pp. 623–670.
[2] Google, X, 2016, "Project Wing," X Development LLC, Mountain View, CA, accessed Jan. 29, 2018, https://x.company/projects/wing/
[3] Deutsche Post Group, 2016, "DHL Parcelcopter 3.0," Deutsche Post AG, Bonn, Germany, accessed Jan. 29, 2018, http://www.dpdhl.com/en/media_relations/specials/parcelcopter.html
[4] Desbiens, A. L., Asbeck, A. T., and Cutkosky, M. R., 2011, "Landing, Perching and Taking Off From Vertical Surfaces," Int. J. Rob. Res., **30**(3), pp. 355–370.
[5] Mellinger, D., Shomin, M., Michael, N., and Kumar, V., 2013, "Cooperative Grasping and Transport Using Multiple Quadrotors," *Distributed Autonomous Robotic Systems* (Springer Tracts in Advanced Robotics, Vol. 83), Springer, Berlin, pp. 545–558.
[6] Graule, M. A., Chirarattananon, P., Fuller, S. B., Jafferis, N. T., Ma, K. Y., Spenko, M., Kornbluh, R., and Wood, R. J., 2016, "Perching and Takeoff of a Robotic Insect on Overhangs Using Switchable Electrostatic Adhesion," Science, **352**(6288), pp. 978–982.
[7] Hawkes, E. W., Jiang, H., and Cutkosky, M. R., 2016, "Three-Dimensional Dynamic Surface Grasping With Dry Adhesion," Int. J. Rob. Res., **35**(8), pp. 943–958.
[8] Yanagimura, K., Ohno, K., Okada, Y., Takeuchi, E., and Tadokoro, S., 2014, "Hovering of MAV by Using Magnetic Adhesion and Winch Mechanisms," IEEE International Conference on Robotics and Automation (ICRA), Hong Kong, China, May 31–June 7, pp. 6250–6257.
[9] Kessens, C. C., Thomas, J., Desai, J. P., and Kumar, V., 2016, "Versatile Aerial Grasping Using Self-Sealing Suction," IEEE International Conference on Robotics and Automation (ICRA), Stockholm, Sweden, May 16–21, pp. 3249–3254.
[10] Gawel, A., Kamel, M., Novkovic, T., Widauer, J., Schindler, D., von Altishofen, B. P., Siegwart, R., and Nieto, J., 2016, "Aerial Picking and Delivery of Magnetic Objects With MAVs," preprint arXiv:1612.02606.
[11] Pope, M. T., Kimes, C. W., Jiang, H., Hawkes, E. W., Estrada, M. A., Kerst, C. F., Roderick, W. R. T., Han, A. K., Christensen, D. L., and Cutkosky, M. R., 2016, "A Multimodal Robot for Perching and Climbing on Vertical Outdoor Surfaces," IEEE Trans. Rob., **33**(1), pp. 38–48.
[12] Lindsey, Q., Mellinger, D., and Kumar, V., 2012, "Construction With Quadrotor Teams," Auton. Rob., **33**(3), pp. 323–336.
[13] Willmann, J., Augugliaro, F., Cadalbert, T., D'Andrea, R., Gramazio, F., and Kohler, M., 2012, "Aerial Robotic Construction Towards a New Field of Architectural Research," Int. J. Archit. Comput., **10**(3), pp. 439–460.
[14] Augugliaro, F., Lupashin, S., Hamer, M., Male, C., Hehn, M., Mueller, M. W., Willmann, J. S., Gramazio, F., Kohler, M., and Andrea, R. D., 2014, "The Flight Assembled Architecture Installation: Cooperative Construction With Flying Machines," IEEE Control Syst., **34**(4), pp. 46–64.
[15] Korpela, C., Orsag, M., and Oh, P., 2014, "Towards Valve Turning Using a Dual-Arm Aerial Manipulator," IEEE/RSJ International Conference on Intelligent Robots and Systems (IROS), Chicago, IL, Sept. 14–18, pp. 3411–3416.
[16] Pounds, P. E. I., Bersak, D. R., and Dollar, A. M., 2011, "Grasping From the Air: Hovering Capture and Load Stability," IEEE International Conference on Robotics and Automation (ICRA), Shanghai, China, May 9–13, pp. 2491–2498.
[17] Doyle, C. E., Bird, J. J., Isom, T. A., Kallman, J. C., Bareiss, D. F., Dunlop, D. J., King, R. J., Abbott, J. J., and Minor, M. A., 2013, "An Avian-Inspired Passive Mechanism for Quadrotor Perching," IEEE/ASME Trans. Mechatronics, **18**(2), pp. 506–517.
[18] Thomas, J., Loianno, G., Daniilidis, K., and Kumar, V., 2016, "Visual Servoing of Quadrotors for Perching by Hanging From Cylindrical Objects," IEEE Rob. Autom. Lett., **1**(1), pp. 57–64.
[19] Chi, W., Low, K. H., Hoon, K. H., and Tang, J., 2014, "An Optimized Perching Mechanism for Autonomous Perching With a Quadrotor," IEEE International Conference on Robotics and Automation (ICRA), Hong Kong, China, May 31–June 7, pp. 3109–3115.
[20] Suseong, K., Seungwon, C., and Kim, H. J., 2013, "Aerial Manipulation Using a Quadrotor With a Two DOF Robotic Arm," IEEE/RSJ International Conference on Intelligent Robots and Systems (IROS), Tokyo, Japan, Nov. 3–7, pp. 4990–4995.
[21] Thomas, J., Polin, J., Sreenath, K., and Kumar, V., 2013, "Avian-Inspired Grasping for Quadrotor Micro UAVs," ASME Paper No. DETC2013-13289.
[22] Huber, F., Kondak, K., Krieger, K., Sommer, D., Schwarzbach, M., Laiacker, M., Kossyk, I., Parusel, S., Haddadin, S., and Albu-Schäffer, A., 2013, "First Analysis and Experiments in Aerial Manipulation Using Fully Actuated Redundant Robot Arm," IEEE/RSJ International Conference on Intelligent Robots and Systems (IROS), Tokyo, Japan, Nov. 3–7, pp. 3452–3457.
[23] Kim, S., Hoseong, S., and Kim, H. J., 2015, "Operating an Unknown Drawer Using an Aerial Manipulator," IEEE International Conference on Robotics and Automation (ICRA), Seattle, WA, May 26–30, pp. 5503–5508.
[24] Kondak, K., Huber, F., Schwarzbach, M., Laiacker, M., Sommer, D., Bejar, M., and Ollero, A., 2014, "Aerial Manipulation Robot Composed of an Autonomous Helicopter and a 7 Degrees of Freedom Industrial Manipulator," 2014 IEEE International Conference on Robotics and Automation (ICRA), Hong Kong, China, May 31–June 7, pp. 2107–2112.
[25] Cano, R., Pérez, C., Pruano, F., Ollero, A., and Heredia, G., 2013, "Mechanical Design of a 6-DOF Aerial Manipulator for Assembling Bar Structures Using UAVs," Workshop on Research, Education and Development of Unmanned Aerial Systems (RED-UAS), Compiegne, France, Nov. 20–22, pp. 1–7.
[26] Melchiorri, C., and Kaneko, M., 2016, "Robot Hands," *Springer Handbook of Robotics*, B. Siciliano and O. Khatib, eds., Springer International Publishing, Cham, Switzerland, pp. 463–480.
[27] Brock, O., Park, J., and Toussaint, M., 2016, "Mobility and Manipulation," *Springer Handbook of Robotics*, B. Siciliano and O. Khatib, eds., Springer International Publishing, Cham, Switzerland, pp. 1007–1036.
[28] Backus, S. B., and Dollar, A. M., 2016, "An Adaptive Three-Fingered Prismatic Gripper With Passive Rotational Joints," IEEE Rob. Autom. Lett., **1**(2), pp. 668–675.
[29] Backus, S. B., Odhner, L. U., and Dollar, A. M., 2014, "Design of Hands for Aerial Manipulation: Actuator Number and Routing for Grasping and Perching," IEEE/RSJ International Conference on Intelligent Robots and Systems (IROS), Chicago, IL, Sept. 14–18, pp. 34–40.
[30] Backus, S. B., and Dollar, A. M., 2017, "Design Optimization of a Prismatic-Revolute-Revolute Joint Hand for Grasping From Unconstrained Vehicles," ASME Paper No. DETC2017-67222.
[31] Lyons, D. M., 1985, "A Simple Set of Grasps for a Dextrous Hand," IEEE International Conference on Robotics and Automation (ICRA), St. Louis, MO, Mar. 25–28, pp. 588–593.
[32] Ma, R. R., Odhner, L. U., and Dollar, A. M., 2013, "A Modular, Open-Source 3D Printed Underactuated Hand," IEEE International Conference on Robotics and Automation (ICRA), Karlsruhe, Germany, May 6–10, pp. 2737–2743.
[33] Calli, B., Walsman, A., Singh, A., Srinivasa, S., Abbeel, P., and Dollar, A. M., 2015, "Benchmarking in Manipulation Research: Using the Yale-CMU-Berkeley Object and Model Set," IEEE Rob. Autom. Mag., **22**(3), pp. 36–52.
[34] Calli, B., Walsman, A., Singh, A., Srinivasa, S., Abbeel, P., and Dollar, A. M., 2015, "Benchmarking in Manipulation Research: The YCB Object and Model Set and Benchmarking Protocols," preprint arXiv:1502.03143.
[35] YCB Benchmarks, 2016, "YCB Benchmarks Main Page," accessed Jan. 29, 2018, http://ycbbenchmarks.org/
[36] Falco, J., Wyk, K. V., Norcross, R., and Messina, E., 2013, "Performance Metrics and Benchmarks to Advance the State of Robotic Grasping," National Institute of Standards and Technology (NIST), Gaithersburg, MD, accessed Jan. 29, 2018, http://www.nist.gov/el/isd/grasp.cfm

Downloaded From: http://mechanismsrobotics.asmedigitalcollection.asme.org/ on 03/02/2018 Terms of Use: http://www.asme.org/about-asme/terms-of-use